Supplemental Material: Identifying a first-order phase transition in neutron star mergers through gravitational waves

Andreas Bauswein,[1,2] Niels-Uwe F. Bastian,[3] David B. Blaschke,[3,4,5] Katerina Chatziioannou,[6] James A. Clark,[7] Tobias Fischer,[3] and Micaela Oertel[8]

[1] *GSI Helmholtzzentrum für Schwerionenforschung, Planckstraße 1, 64291 Darmstadt, Germany*
[2] *Heidelberg Institute for Theoretical Studies, Schloss-Wolfsbrunnenweg 35, 69118 Heidelberg, Germany*
[3] *Institute of Theoretical Physics, University of Wroclaw, 50-205 Wroclaw, Poland*
[4] *National Research Nuclear University (MEPhI), 115409 Moscow, Russia*
[5] *Bogoliubov Laboratory for Theoretical Physics, Joint Institute for Nuclear Research, 141980 Dubna, Russia*
[6] *Canadian Institute for Theoretical Astrophysics, 60 St. George Street, University of Toronto, Toronto, ON M5S 3H8, Canada*
[7] *Center for Relativistic Astrophysics, School of Physics, Georgia Institute of Technology, Atlanta, Georgia 30332, USA*
[8] *LUTH, Observatoire de Paris, PSL Research University, CNRS, Universit Paris Diderot, Sorbonne Paris Cit, 5 place Jules Janssen, 92195 Meudon, France*

(Dated: January 16, 2019)

EQUATIONS OF STATE

We provide here information about the underlying model for the DD2F and the DD2F-SF equations of state (EOSs) as well as the set of candidate EOSs, which serve as a representative sample of purely hadronic EOSs.

The DD2F EOS is based on the relativistic mean-field approach with density dependent couplings [1–3], which is consistent with the EOS constraint derived from an analysis of transverse and elliptic flow data of heavy-ion collision experiments [4, 5]. At low densities and temperatures, the presence of nuclear clusters is taken into account consistently within the modified nuclear statistical equilibrium model of Ref. [6, 7]. DD2F is consistent with all presently known constraints, e.g., neutron matter from chiral effective field theory [8], the nuclear symmetry energy and its slope [9, 10], the maximum mass of nonrotating neutron stars (NSs) [11, 12], and stellar parameters in agreement with the analysis of GW170817 [13–16].

The quark-matter EOS in the high-density regime of DD2F-SF is based on the phenomenological two-flavor string-flip model (SF), derived within the density-functional formalism depending on scalar and vector quark densities (for details see Ref. [17] and references therein). Deconfinement is considered via an effective string potential, which distinguishes SF from common chiral quark-matter approaches, e.g., models of the Nambu-Jona-Lasinio type [18–21] where (de)confinement is absent. A medium-dependent reduction of the string tension is modeled via a Gaussian functional [17]. Divergent quark masses suppress quark degrees of freedom at low densities. The SF model includes an additional dependence on the isovector-vector density, i.e. the equivalent to ρ-meson interactions in hadronic matter [22].

In this work we employ seven different sets of SF parameters [17, 22, 23] listed in Tab. I and we call the resulting EOS models DD2F-SF-n with $n \in \{1, 2, 3, 4, 5, 6, 7\}$. We use the acronym DD2F-SF if we refer to the whole class of all seven hybrid models. In the main article we focus on the exemplary hybrid model DD2F-SF-1, which was also considered in [22]. The SF parameters of our seven quark matter EOSs correspond to different onset and final densities of the first-order phase transition, which are provided in Tab. I (see also Fig. 1). These phase boundaries of DD2F-SF have a mild temperature dependence for the relevant range, e.g., for DD2F-SF-1 at $T = 20$ MeV we have $\rho_{\rm onset} = 2.90 \times \rho_{\rm sat}$ and $\rho_{\rm final} = 3.81 \times \rho_{\rm sat}$ with $\rho_{\rm sat} = 2.7 \times 10^{14}$ g cm^{-3} being the nuclear saturation density (to be compared with the values for $T = 0$ in Tab. I). The first-order phase transition leads to a significant softening of the EOS in the phase transition region, which represents a phase where hadrons and quarks coexist. Vector repulsion, including higher-order terms, in the pure quark matter phase is

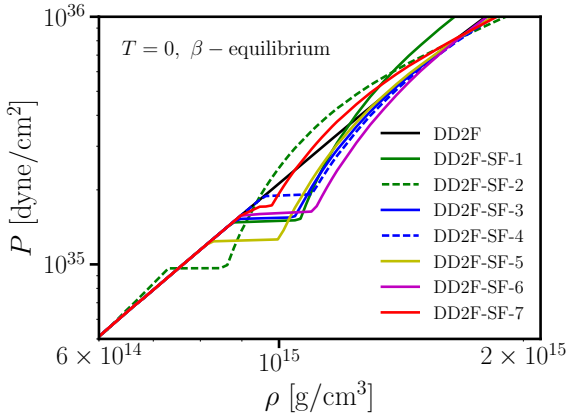

FIG. 1: Pressure as function of the rest-mass density for different hybrid EOSs of the DD2F-SF class. Black curve displays the purely hadronic reference model DD2F.

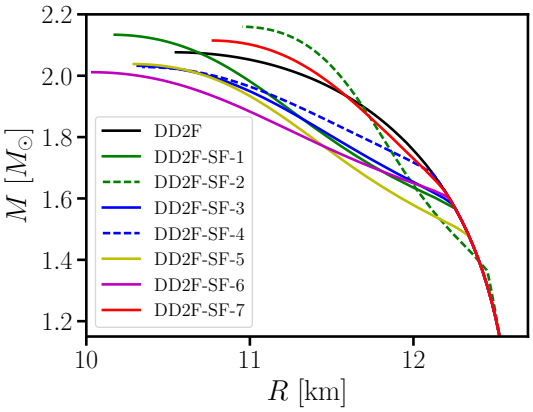

FIG. 2: Mass-radius relations for the DD2F-SF EOSs employed in this study. M is the gravitational mass, R the circumferential eigen radius for nonrotating cold NSs. Solid green (black) curve displays the M-R relation for DD2F-SF-1 (DD2F).

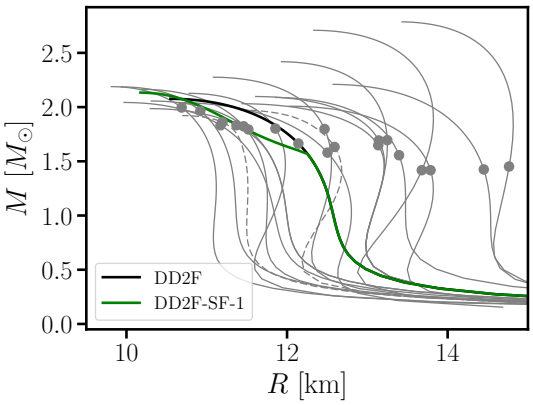

FIG. 3: Mass-radius relations for the model EOSs employed in this study. M is the gravitational mass, R the circumferential eigen radius for nonrotating cold NSs. Green (black) curve displays the M-R relation for DD2F-SF-1 (DD2F). Gray dashed curves correspond to ALF2 and ALF4. Gray dots indicate $M_{\rm fid}$, which corresponds to the stellar configuration whose central rest-mass density equals the maximum density of the early postmerger evolution in a 1.35-1.35 $M_\odot$ simulation with the same EOS.

essential for stable stellar configurations [24, 25]. The chosen SF parameters lead also to a variation of the stiffness of the quark matter EOS (see Fig. 1).

Our parameter choices yield maximum masses for nonrotating stars between 2.01 $M_\odot$ and 2.16 $M_\odot$ for the different DD2F-SF models (see Tab. I). The different properties of the quark phase (onset densities, density jumps and quark phase stiffness) are also apparent in the resulting mass-radius relations of nonrotating cold stars for DD2F-SF, which are shown in Fig. 2 together with the purely hadronic reference model DD2F (black curve). DD2F-SF-1 as reference is indicated by a solid green line. Note that for DD2F-SF-2 we employ a slightly modified variant of the hadronic DD2F which includes an excluded volume modeling [26]. This leads to minor modifications of the hadronic phase just below the onset density (see Figs. 1 and Fig. 2) and is responsible for the slightly larger tidal deformability of DD2F-SF-2 in Fig. 3 of the main paper.

The stellar properties of our reference models DD2F and DD2F-SF-1 are also displayed in Fig. 3. The figure includes mass-radius relations of other EOS models (grey lines), which serve as representative sample of hadronic EOSs in this study. This set includes APR [27], BHBLP [28], BSK20 [29], BSK21 [29], DD2 [2, 6], eosUU [30], GS2 [31], LS220 [32], LS375 [32], NL3 [6, 33], SFHO [34], SFHX [34], Sly4 [35], TM1 [7, 36] and TMA [7, 37] (see [38–40] for the meaning of the acronyms and more details about the different EOSs; GS2, LS375, NL3, TM1 and TMA are incompatible with the 90% credible level of the tidal deformability constraint deduced from GW170817 [13, 15, 16]). Additionally, we consider modified versions of SFHO and DD2 with a 2nd order phase transition to hyperonic matter [41, 42], which we refer to as SFHOY and DD2Y, respectively. Hyperonic interactions for these models have been chosen to be compatible with hypernuclear data and a cold NS maximum mass of 2 $M_\odot$, such that these EOSs fulfill all presently available constraints. We also investigate the two models ALF2 and ALF4 [43, 44] (implemented as piecewise polytropes), which resemble hybrid EOSs with a more continuous transition to quark matter. As discussed in [43] these models (gray dashed curves in Fig. 3) do not show qualitative differences in the mass-radius relations compared to purely hadronic EOSs.

POSTMERGER DENSITIES

In the main article we show that a measurement of the dominant postmerger gravitational-wave (GW) frequency can be used to estimate the highest rest-mass density $\rho_{\rm max}^{\rm max}$ which occurs during the early postmerger evolution (see Fig. 4 in the main article). For softer EOSs higher densities are reached in the postmerger phase. This information can be mapped to nonrotating stellar configurations and roughly determines up to which NS mass the presence of a strong phase transition is probed by the postmerger GW emission of 1.35-1.35 $M_\odot$ binaries as described in the main part.

To this end we identify the nonrotating stellar configuration with a gravitational mass $M_{\rm fid} = M(\rho_{\rm max}^{\rm max})$ whose central rest-mass density equals $\rho_{\rm max}^{\rm max}$. Figure 4 shows $M_{\rm fid}$ as function of $f_{\rm peak}$ for all 1.35-1.35 $M_\odot$ simulations. We also plot $M_{\rm fid}$ as gray dots on the corresponding mass-radius relations of the different EOSs investigated in this

TABLE I: Different hybrid EOS models of the DD2F-SF class employed in this study. D_0, α, a, b, c, ρ_1 are SF parameters as defined in [17, 22, 23]. $n_{\rm onset}$ and Δn are the onset baryon density and baryon density jump of the phase transition (in neutrinoless beta equilibrium and for zero temperature). $M_{\rm onset}$ is the lowest NS mass with a quark matter core. $M_{\rm max}$ is the maximum mass of cold nonrotating NSs. $f_{\rm peak}$ denotes the dominant postmerger GW frequency.

EOS	$\sqrt{D_0}$ (MeV)	α (fm^6)	a (MeV fm^3)	b (MeV fm^9)	c (fm^6)	ρ_1 (MeV fm^3)	$n_{\rm onset}$ (fm^{-3})	Δn (fm^{-3})	$M_{\rm onset}$ ($M_\odot$)	$M_{\rm max}$ ($M_\odot$)	$f_{\rm peak}$ (kHz)
DD2-SF-1	265	0.39	-4.0	1.6	0.025	80.0	0.533	0.106	1.57	2.13	3.54
DD2-SF-2	250	0.60	10.0	0.0	0.000	80.0	0.466	0.057	1.37	2.16	3.68
DD2-SF-3	240	0.36	1.0	0.5	0.015	80.0	0.538	0.094	1.58	2.03	3.58
DD2-SF-4	240	0.34	1.0	0.5	0.015	80.0	0.580	0.082	1.68	2.03	3.36
DD2-SF-5	240	0.38	1.0	0.5	0.015	80.0	0.499	0.108	1.48	2.04	3.59
DD2-SF-6	240	0.30	-3.0	0.8	0.015	80.0	0.545	0.121	1.60	2.01	3.67
DD2-SF-7	240	0.47	7.0	0.2	0.015	80.0	0.562	0.030	1.62	2.11	3.33

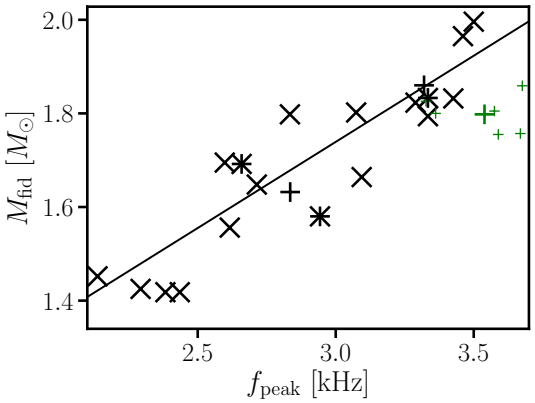

FIG. 4: Gravitational mass $M_{\rm fid}$ of nonrotating NSs whose central rest-mass density equals the maximum rest-mass density $\rho_{\rm max}^{\rm max}$ during the first few milliseconds of the postmerger evolution, for 1.35-1.35 $M_\odot$ mergers producing postmerger GW emission with frequency $f_{\rm peak}$. Green symbols display results for DD2F-SF (big green plus sign for DD2F-SF-1). Solid curve is a second order polynomial least square fit to the data excluding hybrid EOSs. Asterisks mark models with hyperonic matter. Black plus signs indicate ALF2 and ALF4. Models incompatible with GW170817 are not shown.

study. The dots indicate $M_{\rm fid}$ for 1.35-1.35 $M_\odot$ mergers and illustrate which NS mass regime is probed by the postmerger remnant. Events with higher total binary masses $M_{\rm tot}$ would lead to higher densities in the postmerger phase. Consequently, $M_{\rm fid}$ increases with $M_{\rm tot}$.

NEUTRON STAR RADIUS MEASUREMENTS FROM $f_{\rm peak}$

We briefly comment on the empirically found relations between $f_{\rm peak}$ and radii R of a nonrotating NS [38, 45, 46], which can be employed for accurate and robust NS radius measurements under the assumption of purely hadronic EOSs [47–49]. Our results in the main article show that such relations do not generically hold for EOSs with a strong first-order phase transition to quark matter since such models give rise to generally higher frequencies relative to the $f_{\rm peak}(R)$ relation formed by purely hadronic EOSs. This is visible in Fig. 5 for the relation between $f_{\rm peak}$ and the radius of a nonrotating NS with 1.6 $M_\odot$. If there is evidence for the presence of a strong phase transition, a measurement of $f_{\rm peak}$ thus only establishes an accurate lower bound on NS radii. The actual radius may then be up to about 1 km larger than the one inferred from $f_{\rm peak}(R)$ relations of purely hadronic EOSs if the merger remnant contains a large quark matter core as for our 1.35-1.35 $M_\odot$ mergers with DD2F-SF. (The deviation of the DD2F-SF models in $f_{\rm peak}(R)$ relations is larger for $R = R(1.35\ M_\odot)$ and gets smaller for $R = R(1.8\ M_\odot)$ since the latter radius reflects the occurrence of quark matter.)

It is likely that beside the signature uncovered in this work, additional information about the presence of a strong first-order phase transition will become available either by other astronomical measurements (e.g. neutrino signals and other observables of near-by core-collapse supernovae [22]) or by the merger observation itself. For instance, we find that the slope, $\frac{df_{\rm peak}}{dM_{\rm tot}}$, for mergers involving quark matter like the DD2F-SF is significantly steeper compared to the slope of purely hadronic models with comparable $f_{\rm peak}$ (cf. Fig. 1 in Ref. [40]). Here we compare DD2F-SF-1 and the hadronic models APR [27], eosUU [30] and SLy4 [35], which lead to peak frequencies in the range between 3.54 and 3.43 kHz for $M_{\rm tot} = 2.7\ M_\odot$. For DD2F-SF-1, the slope [50] equals 3.6 kHz/$M_\odot$ compared to 0.55 kHz/$M_\odot$, 0.28 kHz/$M_\odot$ and 1.56 kHz/$M_\odot$ for APR, eosUU and SLy4. Observationally, the determination of $\frac{df_{\rm peak}}{dM_{\rm tot}}$ requires two measurements of $f_{\rm peak}$ for different binary masses [40].

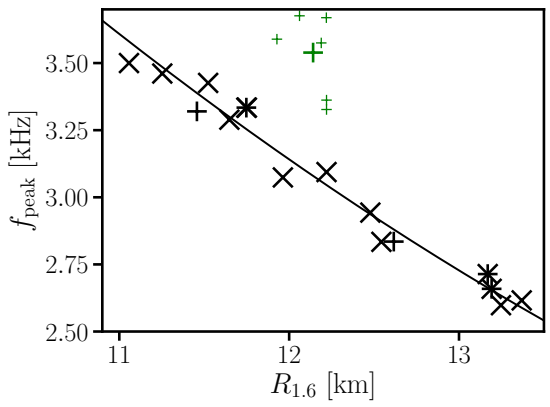

FIG. 5: Dominant postmerger GW frequency $f_{\rm peak}$ as function of the radius $R_{1.6}$ of a nonrotating NS with 1.6 $M_\odot$ for 1.35-1.35 $M_\odot$ binaries. The DD2F-SF models are shown by green symbols (big green plus sign for DD2F-SF-1). Asterisks mark hyperonic EOSs. Black plus signs indicate ALF2 and ALF4. The solid curve provides a second order polynomial least square fit to the data (black symbols, excluding hybrid EOSs). Models incompatible with GW170817 are not shown.

[1] S. Typel, Phys. Rev. C **71**, 064301 (2005).
[2] S. Typel, G. Röpke, T. Klähn, D. Blaschke, and H. H. Wolter, Phys. Rev. C **81**, 015803 (2010).
[3] D. Alvarez-Castillo, A. Ayriyan, S. Benic, D. Blaschke, H. Grigorian, and S. Typel, European Physical Journal A **52**, 69 (2016).
[4] P. Danielewicz, R. Lacey, and W. G. Lynch, Science **298**, 1592 (2002).
[5] C. Y. Tsang, M. B. Tsang, P. Danielewicz, W. G. Lynch, and F. J. Fattoyev, ArXiv e-prints (2018), 1807.06571.
[6] M. Hempel and J. Schaffner-Bielich, Nucl. Phys. A **837**, 210 (2010).
[7] M. Hempel, T. Fischer, J. Schaffner-Bielich, and M. Liebendörfer, Astrophys. J. **748**, 70 (2012).
[8] T. Krüger, I. Tews, K. Hebeler, and A. Schwenk, Phys. Rev. C **88**, 025802 (2013).
[9] J. M. Lattimer and Y. Lim, Astrophys. J. **771**, 51 (2013).
[10] M. Oertel, M. Hempel, T. Klähn, and S. Typel, Reviews of Modern Physics **89**, 015007 (2017).
[11] J. Antoniadis, P. C. C. Freire, N. Wex, T. M. Tauris, R. S. Lynch, M. H. van Kerkwijk, M. Kramer, C. Bassa, V. S. Dhillon, T. Driebe, et al., Science **340**, 448 (2013).
[12] Z. Arzoumanian, A. Brazier, S. Burke-Spolaor, S. Chamberlin, S. Chatterjee, B. Christy, J. M. Cordes, N. J. Cornish, F. Crawford, H. Thankful Cromartie, et al., Astrophys. J. Supp. **235**, 37 (2018).
[13] B. P. Abbott, R. Abbott, T. D. Abbott, F. Acernese, K. Ackley, C. Adams, T. Adams, P. Addesso, R. X. Adhikari, V. B. Adya, et al. (LIGO Scientific Collaboration and Virgo Collaboration), Phys. Rev. Lett. **119**, 161101 (2017).
[14] A. Bauswein, O. Just, H.-T. Janka, and N. Stergioulas, Astrophys. J. Lett. **850**, L34 (2017).
[15] S. De, D. Finstad, J. M. Lattimer, D. A. Brown, E. Berger, and C. M. Biwer, Phys. Rev. Lett. **121**, 091102 (2018).
[16] B. P. Abbott, R. Abbott, T. D. Abbott, F. Acernese, K. Ackley, C. Adams, T. Adams, P. Addesso, R. X. Adhikari, V. B. Adya, et al., Phys. Rev. Lett. **121**, 161101 (2018).
[17] M. A. R. Kaltenborn, N.-U. F. Bastian, and D. B. Blaschke, Phys. Rev. D **96**, 056024 (2017).
[18] Y. Nambu and G. Jona-Lasinio, Phys. Rev. **122**, 345 (1961).
[19] S. Klevansky, Rev. Mod. Phys. **64**, 649 (1992).
[20] S. B. Rüster, V. Werth, M. Buballa, I. A. Shovkovy, and D. H. Rischke, Phys. Rev. D **72**, 034004 (2005).
[21] D. Blaschke, S. Fredriksson, H. Grigorian, A. M. Öztaş, and F. Sandin, Phys. Rev. D **72**, 065020 (2005).
[22] T. Fischer, N.-U. F. Bastian, M.-R. Wu, P. Baklanov, E. Sorokina, S. Blinnikov, S. Typel, T. Klähn, and D. B. Blaschke, Nature Astronomy **2**, 980 (2018).
[23] N.-U. Bastian, D. Blaschke, T. Fischer, and G. Röpke, Universe **4**, 67 (2018).
[24] S. Benic, D. Blaschke, D. E. Alvarez-Castillo, T. Fischer, and S. Typel, Astron. Astrophys. **577**, A40 (2015).
[25] T. Klähn and T. Fischer, Astrophys. J. **810**, 134 (2015).
[26] S. Typel, European Physical Journal A **52**, 16 (2016).
[27] A. Akmal, V. R. Pandharipande, and D. G. Ravenhall, Phys. Rev. C **58**, 1804 (1998).
[28] S. Banik, M. Hempel, and D. Bandyopadhyay, Astrophys. J. Supp. **214**, 22 (2014).
[29] S. Goriely, N. Chamel, and J. M. Pearson, Phys. Rev. C **82**, 035804 (2010).
[30] R. B. Wiringa, V. Fiks, and A. Fabrocini, Phys. Rev. C **38**, 1010 (1988).
[31] G. Shen, C. J. Horowitz, and S. Teige, Phys. Rev. C **83**, 035802 (2011).
[32] J. M. Lattimer and F. Douglas Swesty, Nuclear Physics A **535**, 331 (1991).
[33] G. A. Lalazissis, J. König, and P. Ring, Phys. Rev. C **55**, 540 (1997).
[34] A. W. Steiner, M. Hempel, and T. Fischer, Astrophys. J. **774**, 17 (2013).
[35] F. Douchin and P. Haensel, Astron. Astrophys. **380**, 151 (2001).
[36] Y. Sugahara and H. Toki, Nuclear Physics A **579**, 557 (1994).
[37] H. Toki, D. Hirata, Y. Sugahara, K. Sumiyoshi, and I. Tanihata, Nuclear Physics A **588**, 357 (1995).
[38] A. Bauswein, H.-T. Janka, K. Hebeler, and A. Schwenk, Phys. Rev. D **86**, 063001 (2012).
[39] A. Bauswein, S. Goriely, and H.-T. Janka, Astrophys. J. **773**, 78 (2013).
[40] A. Bauswein, N. Stergioulas, and H.-T. Janka, Phys. Rev. D **90**, 023002 (2014).
[41] M. Fortin, M. Oertel, and C. Providência, Publications of the Astronomical Society of Australia **35** (2018).
[42] M. Marques, M. Oertel, M. Hempel, and J. Novak, Phys. Rev. **C96**, 045806 (2017).
[43] M. Alford, M. Braby, M. Paris, and S. Reddy, Astrophys. J. **629**, 969 (2005).
[44] J. S. Read, B. D. Lackey, B. J. Owen, and J. L. Friedman, Phys. Rev. D **79**, 124032 (2009).
[45] A. Bauswein and H.-T. Janka, Phys. Rev. Lett. **108**, 011101 (2012).

[46] K. Hotokezaka, K. Kiuchi, K. Kyutoku, T. Muranushi, Y. Sekiguchi, M. Shibata, and K. Taniguchi, Phys. Rev. D **88**, 044026 (2013).

[47] J. Clark, A. Bauswein, L. Cadonati, H.-T. Janka, C. Pankow, and N. Stergioulas, Phys. Rev. D **90**, 062004 (2014).

[48] J. A. Clark, A. Bauswein, N. Stergioulas, and D. Shoemaker, Classical and Quantum Gravity **33**, 085003 (2016).

[49] K. Chatziioannou, J. A. Clark, A. Bauswein, M. Millhouse, T. B. Littenberg, and N. Cornish, Phys. Rev. D **96**, 124035 (2017.

[50] We determine $\frac{df_{\rm peak}}{dM_{\rm tot}}$ by $(f_{\rm peak}(2.7\,M_\odot) - f_{\rm peak}(2.6\,M_\odot))/0.1M_\odot$.